International Journal of Research in Engineering and Science (IJRES)
ISSN (Online): 2320-9364, ISSN (Print): 2320-9356
www.ijres.org Volume 14 Issue 4 ǁ April 2026 ǁ PP. 119-126

Effect of heat treatment on the microstructure and mechanical properties of laser powder bed fusion Mar-M247 alloy

Junbin Zhou[1]
[1] *School of Materials and Chemistry, University of Shanghai for Science and Technology, Shanghai 200093, China*

Abstract
This study investigates the microstructural characteristics and mechanical behavior of Mar-M247 nickel-based superalloy fabricated via laser powder bed fusion (LPBF) in the heat-treated state. The microstructural investigation focuses on the morphology, size distribution, and spatial arrangement of the secondary γ′ precipitates within the γ matrix, as well as the grain boundary features. Electron backscatter diffraction (EBSD) analysis was employed to characterize the grain structure, crystallographic orientation, and misorientation distribution. The mechanical performance, specifically the tensile properties and microhardness, was evaluated and correlated with these microstructural constituents. The results show that the mechanical response is closely governed by the interaction between the dislocations and the refined γ′ precipitates. Furthermore, the influence of the hierarchical grain structure and the distribution of alloying elements on the deformation stability was discussed. This work provides a comprehensive dataset and fundamental understanding of the microstructural-mechanical correlations in heat-treated LPBF Mar-M247 alloy, contributing to the establishment of performance standards for additively manufactured high-temperature components.

Keywords: *Mar-M247 alloy, Laser powder bed fusion (LPBF), Microstructure, Mechanical properties, Heat treatment.*

Date of Submission: 09-04-2026 Date of Acceptance: 22-04-2026

I. INTRODUCTION

Mar-M247 is a γ′-phase Ni_3(Al, Ti) precipitation-strengthened nickel-based superalloy, characterized by a high γ′-phase volume fraction of approximately 62% [1–3]. Nickel-based precipitation-strengthened superalloys[3–6], such as Mar-M247, have become indispensable materials for the hot-section components of aero-engines and gas turbines, owing to their exceptional high-temperature creep strength, superior oxidation resistance, and microstructural stability [7–9]. The performance of these alloys is primarily attributed to the high volume fraction of γ′-phase precipitates Ni3(Al, Ti) dispersedly distributed within the γ matrix [10]. With the rapid advancement of additive manufacturing (AM) technologies [11,12], laser powder bed fusion (LPBF) offers a promising route for the net-shape fabrication of high-performance turbine components[13–17], due to its unique advantages in producing complex geometries and thin-walled structures [18].

However, due to the high cooling rates during the LPBF process, the microstructure of as-LPBF samples is in a metastable state. Consequently, as- LPBF samples cannot be used directly, and their microstructural stability must be enhanced through heat treatment. Currently, as- LPBF samples are typically treated with a combination of various heat treatment methods, such as stress relief annealing, hot isostatic pressing (HIP), solution treatment, and aging treatment [19–21]. These methods have been reported to contribute to the improvement of the mechanical properties of superalloys. For instance, after HIP treatment, the columnar grains in LPBF-fabricated CM247LC alloy transformed into equiaxed grains, with the γ′ phase uniformly distributed at the grain boundaries, leading to an increase in tensile strength from 1140 MPa to 1457 MPa [22]. Furthermore, studies have investigated the effects of HIP+SA treatment at different solution temperatures (1205–1245 °C) on the γ′ phase [23]. The results indicated that as the solution temperature increased, the quantity of the γ′ phase increased significantly, while its size decreased.

This study focuses on a comparative analysis of the microstructural evolution and mechanical properties of Mar-M247 alloy fabricated by laser powder bed fusion (LPBF) under two processing routes: "remelting + heat treatment" and "without remelting + heat treatment". Through comparative analysis, emphasis is placed on examining the modification effect of heat treatment on the as-built non-equilibrium microstructure (e.g., segregation, columnar grains, and sub-micron cellular structures) and the subsequent precipitation characteristics

of the primary γ′ strengthening phase. This research aims to establish the intrinsic correlation between microstructural evolution and mechanical response, providing experimental insights into the phase transformation behavior of this alloy under additive manufacturing thermal cycles and subsequent heat treatments.

II. MATERIALS AND METHODS

2.1 Materials and sample fabrication

In this study, spherical gas-atomized Mar-M247 alloy powder was employed, with particle size distributions of D10 = 30.5 μm, D50 = 43.1 μm, and D90 = 61.1 μm (Fig. 1a). The chemical composition of the Mar-M247 powder is listed in (b) **dimensions of tensile test specimens.**

Table 1. LPBF Mar-M247 specimens were fabricated using an EOS M290 system (EOS GmbH, Germany) under an argon shielding atmosphere, with the oxygen content strictly controlled below 900 ppm. To minimize thermal gradients and residual stresses during fabrication, the substrate was preheated to 150°C. Following parameter optimization via the Doehlert matrix method, the finalized manufacturing parameters were set as follows: (1) without remelting samples: laser power of 130 W, scanning speed of 1366 mm/s, hatch spacing of 0.05 mm, and layer thickness of 20 μm; (2) remelting samples (the scanning path remains identical for two consecutive scans): initial exposure parameters: laser power of 130 W, scanning speed of 1366 mm/s, hatch spacing of 0.05 mm, and layer thickness of 20 μm and secondary exposure parameters: laser power of 148.5 W, scanning speed of 1300 mm/s, hatch spacing of 0.06 mm, and layer thickness of 20 μm. All specimens adopted a stripe scanning strategy with a 67° rotation between adjacent layers in the LPBF process. Heat treatment methods used on the specimens was hot isostatic pressing (HIP, 1240 ℃ and 150 MPa × 2 h/furnace cooling), solution treatment (1260 ℃ × 2 h/air cooling) and aging treatment (871 ℃ × 2 h/air cooling).

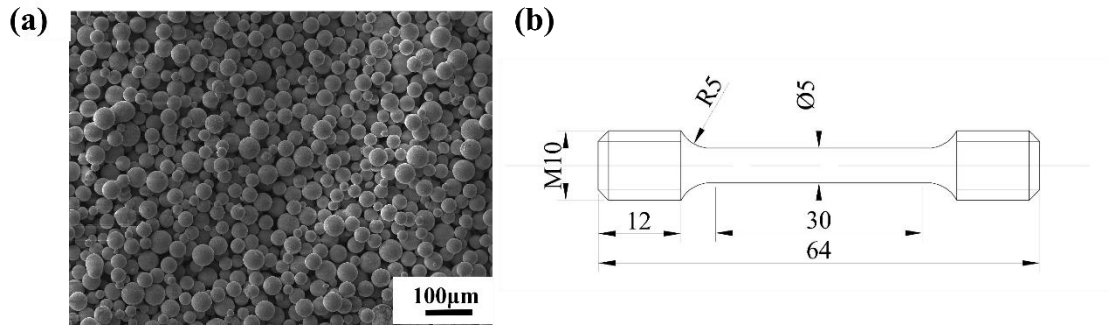

Fig. 1 (a) Powder morphologies; (b) dimensions of tensile test specimens.

Table 1 Chemical element composition of LPBF Mar-M247 alloy (wt.%).

C	Cr	Co	W	Mo	Hf	Al	Ti	Ta	B	Zr	Ni
0.15	8.46	9.82	9.85	0.68	1.58	5.52	1.02	3.1	0.014	0.039	Bal.

2.2 Experimental methods

To investigate the microstructural evolution of the heat-treated LPBF Mar-M247 alloy, specimens were initially prepared through coarse and fine grinding using SiC paper (from 220# to 5000#), followed by polishing with a SiO_2 suspension. Subsequently, backscattered electron (BSE) micrographs were acquired using a ZEISS Gemini SEM300 to observe the microstructural evolution before and after heat treatment. Energy-dispersive X-ray spectroscopy (EDS) was employed for qualitative elemental analysis of the microstructures. The operating parameters for BSE imaging included an acceleration voltage of 15 kV, a probe current of 15 nA, and a working distance of 10 mm.

Furthermore, electron backscattered diffraction (EBSD) equipped on the ZEISS Gemini SEM300 was utilized to characterize the grain size, crystallographic orientation, and texture intensity of the LPBF Mar-M247

alloy. Post-processing of the EBSD data was primarily conducted using Aztec Crystal and TSL-OIM Analysis software to analyze grain size, dislocation distribution, grain boundary types, and the fraction and types of twins. To evaluate the tensile properties, tensile specimens were machined via wire electrical discharge machining (WEDM) into a dog-bone shape with a nominal width of 6 mm and a gauge length of 70 mm, in accordance with the ASTM E8/E8M-22 standard (USA) (Fig. 1b). A strain rate of 0.005 mm/mm/min was applied until the yield point, after which the loading rate was adjusted to 3–5 mm/min until fracture. Finally, the fracture surfaces of the tensile specimens were characterized using a TESCAN VEGA3 tungsten filament scanning electron microscope (SEM) operating at an acceleration voltage of 10 kV, a probe current of 10 nA, and a working distance of 10–25 mm.

III. RESULT AND DISCUSSION

3.1. Initial Microstructure in the As-built State

At low magnification, the as-deposited LPBF Mar-M247 alloy exhibits a distinctive melt pool morphology in the fabrication direction (XZ cross-section), which differs from the conventional "fish-scale" pattern typical of standard manufacturing (Fig. 2a). Under higher magnification, the XZ cross-section reveals refined dendrites and honeycomb-like cellular structures (Fig. 2b), a direct consequence of the ultra-high cooling rates inherent to the LPBF process. Concurrently, due to the steep thermal gradients generated during LPBF, dendrites tend to grow from the build platform toward the melt pool boundaries, often epitaxially extending across multiple melt pools (Fig. 2b). Furthermore, the inhomogeneous distribution of Ta and Hf elements during rapid solidification leads to their segregation at grain boundaries, eventually resulting in the precipitation of blocky MC carbides during the final stages of solidification (Fig. 3).

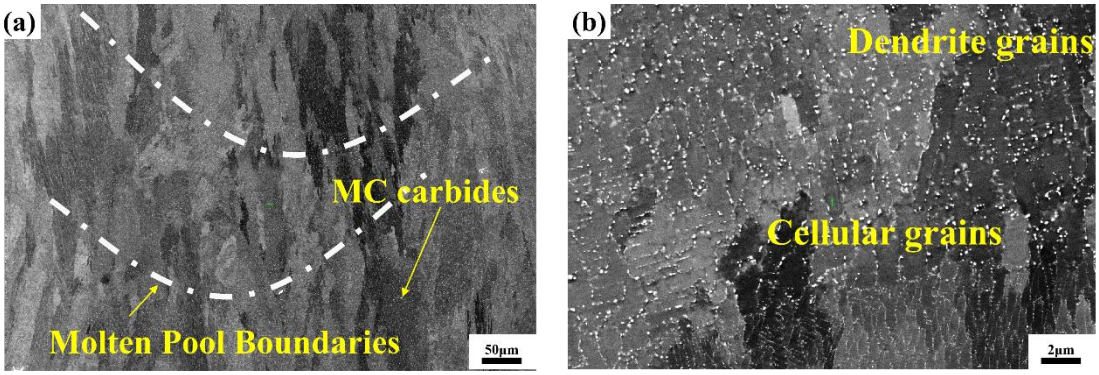

Fig. 2 Characterization of the microstructure of the XZ section of LPBF Mar-M247 alloy in the as-built state (a) microstructure at low magnification; (b) microstructure at high magnification.

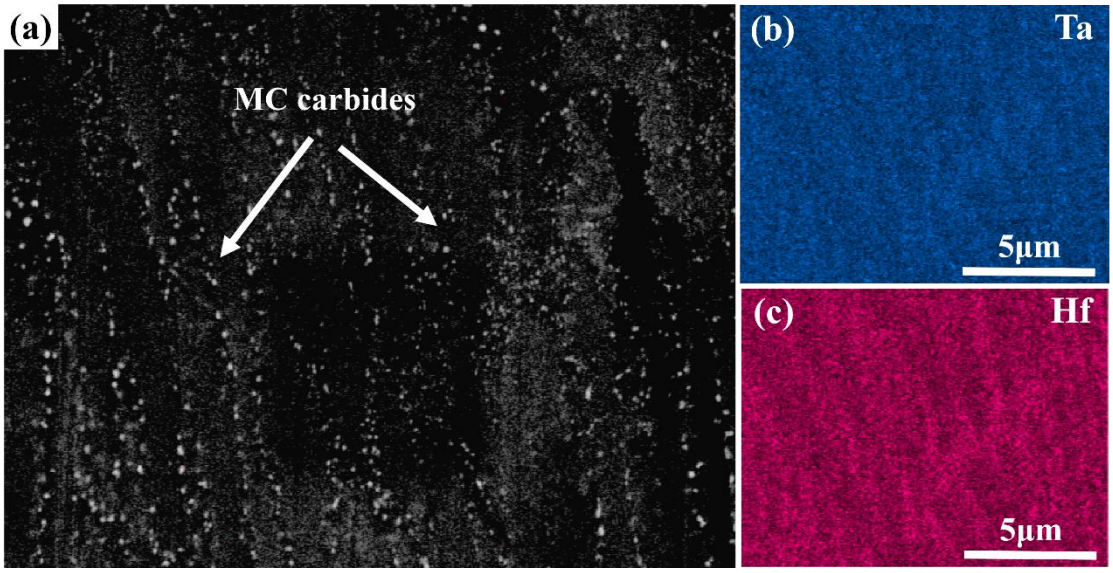

Fig. 3 Characterization of precipitated phase in XZ section of LPBF Mar-M247 alloy in the as-built state.

The EBSD results, as depicted in the Inverse Pole Figure (IPF) maps, reveal that the microstructure of the as-deposited LPBF Mar-M247 alloy is composed of a large number of elongated columnar grains and fine

equiaxed grains, with an average grain size of 10.80 ± 3.01 μm (Fig. 4a and c). In addition, for the as-built LPBF Mar-M247 specimens, high-angle grain boundaries (HAGBs) primarily occur between adjacent columnar grains growing along the build direction, whereas low-angle grain boundaries (LAGBs) are predominantly distributed within the interior of these columnar grains (Fig. 4b).Furthermore, as the growth direction of columnar grains is typically anti-parallel to the direction of heat flow, a predominant <001> texture parallel to the building direction (BD) is observed in the as-deposited alloy. The corresponding texture intensity and texture index are 14.60 and 5.74, respectively (Fig. 4d).

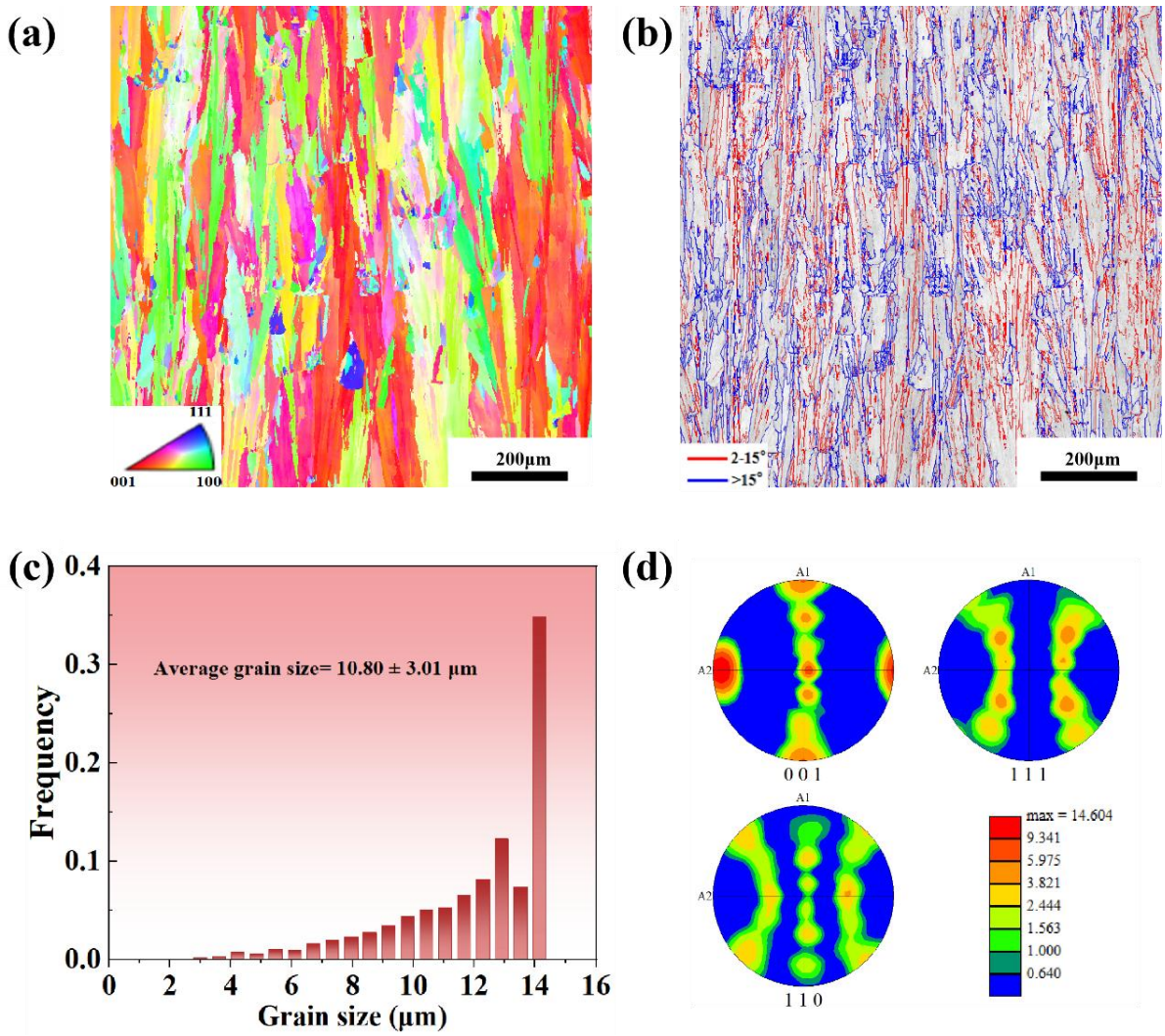

Fig. 4 Analysis of the EBSD results of the as-built LPBF Mar-M247 alloy in XZ cross-section (a) inverse pole figure mapping; (b) grain boundary type image (where low angle boundaries are shown as red lines and high angle boundaries are shown as blue lines); (c) average grain size statistics image; and (d) as-built state pole figure mapping (A1 // BD, A2 // TD).

3.2. Microstructural Evolution during Heat Treatment

Post-thermal processing via HIP+SA induced a significant reconfiguration of the LPBF Mar-M247 grain structure. As shown in Fig. 5a, the characteristic "fish-scale" melt pool boundaries and the metastable sub-micron cellular substructures inherent to the as-built state were completely dissolved. In their place, a coarsened columnar grain morphology emerged, interspersed with regions of partial recrystallization. This limited recrystallization is primarily attributed to the high thermal stability of the Mar-M247 alloy, whose recrystallization temperature resides above the current heat treatment setpoint. Consequently, the alloy retains a degree of the hierarchical grain structure inherited from the LPBF process, while achieving a more stable equilibrium state.

The high-temperature environment during HIP serves as a potent driving force for multi-elemental atomic diffusion, which is critical for defect remediation. Elemental mapping (Fig. 5c) reveals that solute elements such as Hf and Ta, which were heavily sequestered at crack tips due to rapid solidification, diffused toward solute-depleted regions. This homogenization effectively mitigated the chemical gradients and eliminated the stress

concentrations that traditionally trigger crack propagation. More importantly, this diffusion facilitates the closure of micro-gaps, enabling a transition from mechanical interlocking to robust metallurgical bonding at the previous crack interfaces. The subsequent precipitation of blocky MC-type carbides at these interfaces further acts as a "micro-bridge," significantly enhancing the interfacial cohesive strength and ensuring structural integrity.

Quantitative microstructural analysis confirms a highly controlled precipitation of the γ′ strengthening phase following aging treatment (Fig. 5b). The γ′ precipitates exhibit a homogeneous cubic morphology with an average size of 150 ± 30 nm and a narrow size distribution (120–180 nm), achieving a substantial volume fraction of 58%. From a micromechanical perspective, the potency of γ′ strengthening is intrinsically linked to the dislocation interaction mode. Within the 100–200 nm size regime, the precipitates effectively impede dislocation motion via the Orowan looping mechanism. Instead of shearing through the particles, dislocations are forced to bow around the γ′ precipitates, leaving behind dislocation loops that provide a significant increment in flow stress. The synergy between optimized γ′ size and high-volume fraction constitutes the primary physical basis for the superior high-temperature strength observed in the post-treated Mar-M247 alloy.

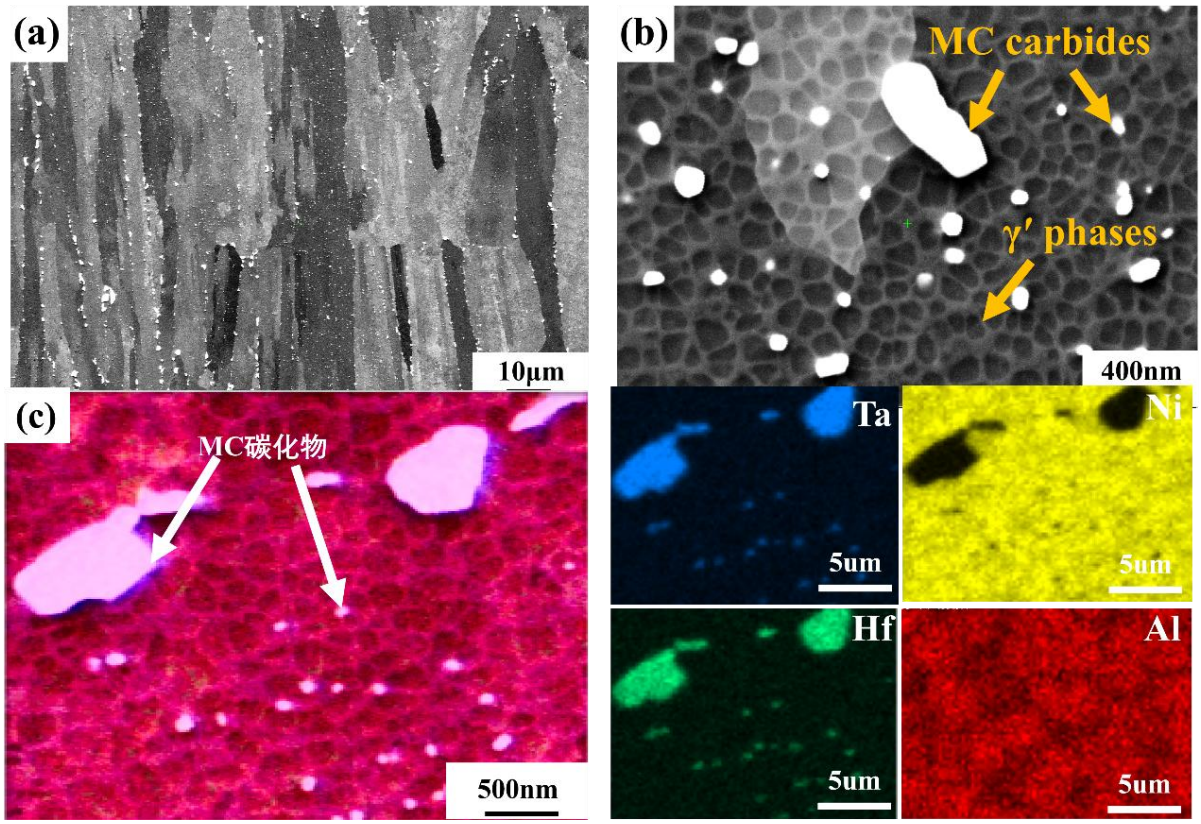

Fig. 5 Microstructure of LPBF Mar-M247 alloy after HIP+SA treatment (a) low magnification microstructure image; (b) high magnification microstructure image; (c) Carbide EDS analysis.

Due to the occurrence of only partial recrystallization, the anisotropy within the LPBF Mar-M247 alloy persists following the heat treatment, with the <001> fiber texture remaining dominant (Fig. 6a). Nevertheless, notable grain growth is observed, with the average grain size increasing from 10.80 μm to 10.84 μm (Fig. 6b). Furthermore, a comparative analysis of the Grain Boundary Character Distribution (GBCD) reveals that the fraction of High-Angle Grain Boundaries (HAGBs) decreased from 43.5% to 22.4%, whereas the proportion of Low-Angle Grain Boundaries (LAGBs) increased from 56.5% to 77.6% (Fig. 6c). Additionally, no significant annealing twin boundaries were detected in the LPBF Mar-M247 alloy after the HIP+SA treatment (Fig. 6a and 6c). The Pole Figures (PFs) further exhibit a mitigation in crystallographic orientation intensity, with the maximum texture intensity decreasing from 16.84 to 12.85 and the texture index dropping from 5.84 to 5.14 (Fig. 6d). These results demonstrate that while recrystallization remains incomplete, the grain orientation of the alloy was effectively weakened, indicating that the thermal treatment partially relieved the strong preferential orientation induced by the rapid solidification inherent to the LPBF process.

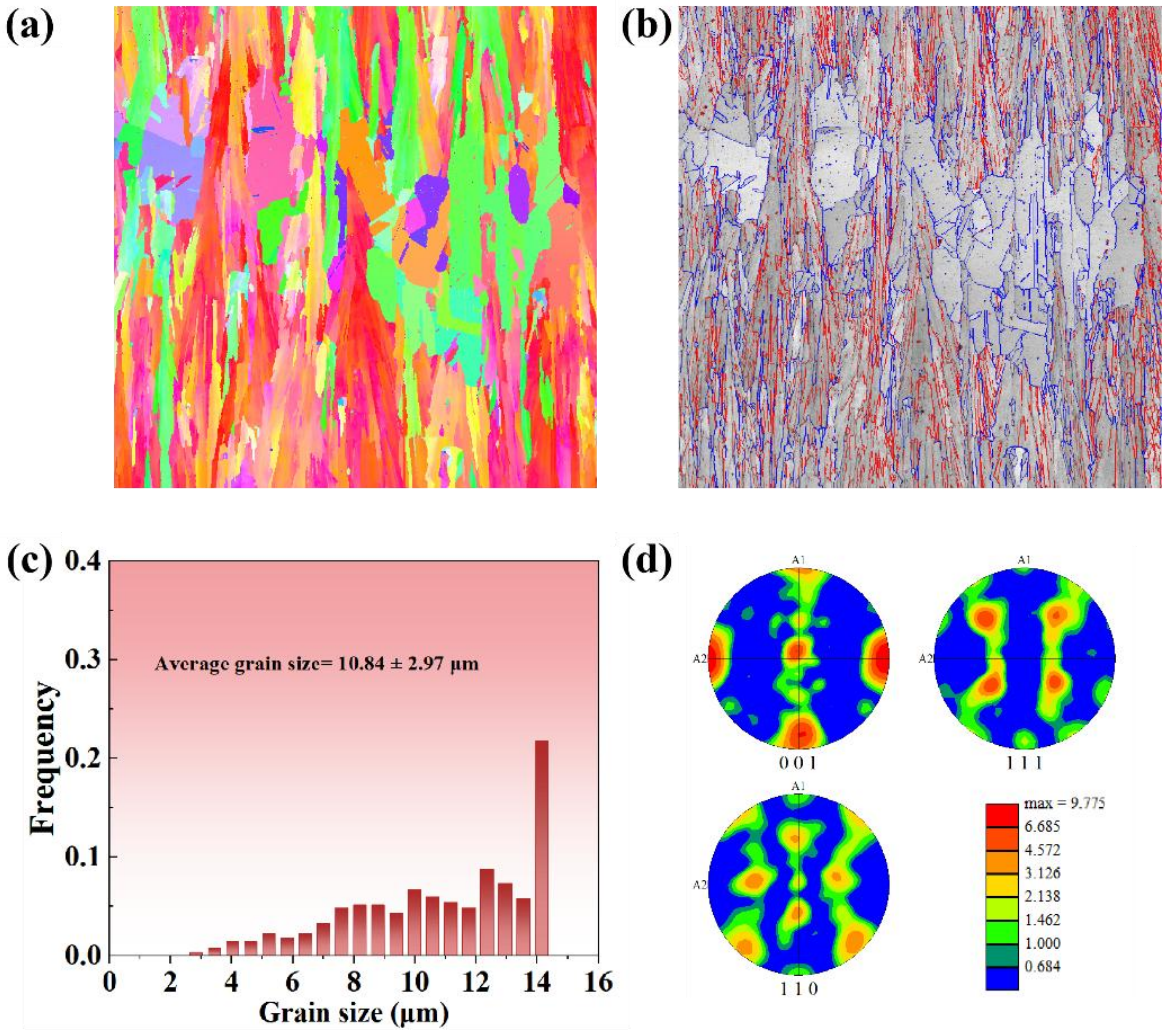

Fig. 6 Analysis of EBSD results of HIP+SA treated LPBF Mar-M247 alloy in XZ cross-section (a) inverse pole figure mapping; (b) plot of grain boundary types (where small-angle boundaries are shown as red line segments, and large-angle boundaries are shown as blue line segments); (c) statistical plot of average grain size and (d) heat-treated state pole figure mapping.

3.3 Mechanical Properties of LPBF Mar-M247 Alloy

The room-temperature tensile tests indicate that the mechanical properties of the LPBF Mar-M247 alloy were significantly enhanced following the HIP+SA treatment (Fig. 7). Due to the uniform intragranular precipitation of the γ′ phase, the yield strength (YS) of the alloy increased from 892 MPa to 1016 MPa (an improvement of 1.14%), and the ultimate tensile strength (UTS) rose from 1130 MPa to 1213 MPa (an improvement of 1.07%) (Fig. 7). Furthermore, the effective elimination of micro-cracks during the HIP process resulted in a substantial increase in elongation (EL), which rose from 6.4 % to 8.9 % (a 39% improvement) (Fig. 7). The tensile data for each condition reported above were obtained from at least three valid specimens (n=3).

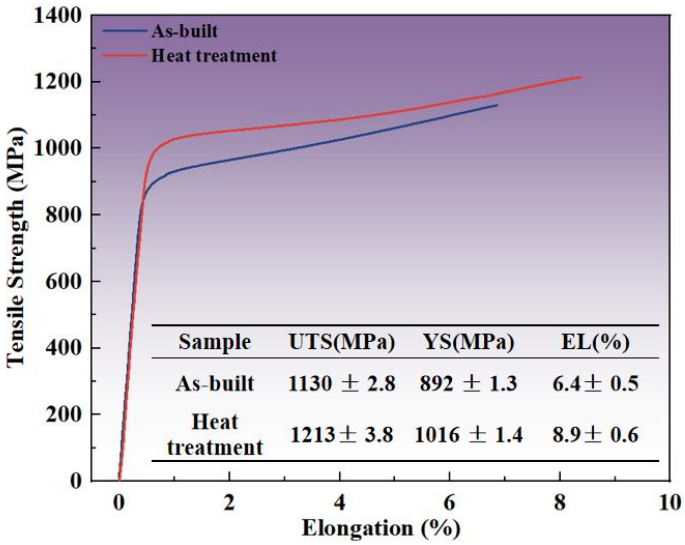

Fig. 7 Tensile properties of LPBF Mar-M247 alloy: Stress-strain image before and after heat treatment

IV. CONCLUSION

This study investigated the effects of post-thermal processing on the microstructural evolution and tensile properties of laser powder bed fusion (LPBF) Mar-M247 alloy, with a specific focus on the correlation between γ′ precipitates, MC carbides, and strengthening mechanisms. Microstructural Characteristics of As-built Alloy: The as-deposited LPBF Mar-M247 alloy exhibited a characteristic "fish-scale" melt pool morphology at low magnification, while refined cellular and dendritic structures were observed at higher magnification. This distinctive microstructure originates from the steep thermal gradients inherent to the LPBF process. During rapid solidification, grains grew preferentially anti-parallel to the heat flow direction, leading to epitaxial growth of columnar grains across multiple melt pools and the formation of a strong <001> crystallographic texture. Simultaneously, significant micro-segregation of Hf and Ta at the dendritic and cellular boundaries triggered the extensive precipitation of MC carbides, which initially compromised the overall mechanical integrity of the as-built alloy. Microstructural Reconfiguration post-HIP+SA: Following the HIP+SA treatment, the "fish-scale" melt pool boundaries were dissolved, and the alloy underwent partial recrystallization, where the primary cellular/dendritic structures were replaced by coarsened columnar grains. The average grain size increased from 10.80 μm to 10.84 μm. Despite the incomplete recrystallization, the dominant <001> texture was largely retained. Furthermore, a high density of blocky MC carbides dispersedly precipitated along the grain boundaries, while a substantial volume fraction of granular γ′ phases was uniformly distributed within the γ matrix. These microstructural modifications were instrumental in enhancing the alloy's strength. Enhancement of Mechanical Performance: Comparative mechanical analysis revealed that the HIP+SA treatment significantly elevated the overall performance of the LPBF Mar-M247 alloy. Notably, both the tensile strength and elongation exhibited a substantial increase compared to the as-deposited state, demonstrating a superior synergy between strength and ductility.

REFERENCES

[1]. Milenkovic, S., Sabirov, I. & Llorca, J. Effect of the cooling rate on microstructure and hardness of MAR-M247 Ni-based superalloy. Mater. Lett. 73, 216–219 (2012).
[2]. Azevedo e Silva, P. R. S., Baldan, R., Nunes, C. A., Coelho, G. C. & Costa, A. M. da S. Solution heat-treatment of Nb-modified MAR-M247 superalloy. Mater. Charact. 75, 214–219 (2013).
[3]. Hagedorn, Y.-C. et al. Processing of nickel based superalloy MAR M-247 by means of High Temperature - Selective Laser Melting (HT - SLM). 291–295 (2014).
[4]. Kunz, L., Lukáš, P. & Konečná, R. High-cycle fatigue of Ni-base superalloy Inconel 713LC. Int. J. Fatigue 32, 908–913 (2010).
[5]. Amato, K. N. et al. Microstructures and mechanical behavior of Inconel 718 fabricated by selective laser melting. Acta Mater. 60, 2229–2239 (2012).
[6]. Engeli, R., Etter, T., Hövel, S. & Wegener, K. Processability of different IN738LC powder batches by selective laser melting. J. Mater. Process. Technol. 229, 484–491 (2016).
[7]. Jena, A., Atabay, S. E., Gontcharov, A. B., Lowden, P. & Brochu, M. Laser Powder Bed Fusion of a New High gamma prime Ni-based Superalloy with Improved Weldability. Mater. Des. 208, 109895 (2021).
[8]. Sanchez, S. et al. Powder Bed Fusion of nickel-based superalloys: A review. Int. J. Mach. Tools Manuf. 165, 103729 (2021).
[9]. Bosque, A., Fernández-Arias, P. & Vergara, D. Advances in the Additive Manufacturing of Superalloys. Journal of Manufacturing and Materials Processing vol. 9 215 at https://doi.org/10.3390/jmmp9070215 (2025).
[10]. Panwisawas, C., Tang, Y. T. & Reed, R. C. Metal 3D printing as a disruptive technology for superalloys. Nat. Commun. 11, 1–4 (2020).

[11]. Wu, D. et al. Analysis of the intermediate temperature brittleness of LPBF-fabricated Ni-based alloys with high γ′ phase fraction. Mater. Sci. Eng. A 953, 149713 (2026).
[12]. Xu, J., Kontis, P., Peng, R. L. & Moverare, J. Modelling of additive manufacturability of nickel-based superalloys for laser powder bed fusion. Acta Mater. 240, 118307 (2022).
[13]. Liu, L. et al. Crack inhibition to enhance strength-ductility of CM247LC alloy fabricated by laser powder bed fusion. Mater. Sci. Eng. A 875, 145114 (2023).
[14]. Zhou, L. et al. The evolution of microstructure and mechanical properties of Inconel 625 alloy fabricated by laser powder bed fusion via novel hybrid scanning strategy. Mater. Sci. Eng. A 911, 146925 (2024).
[15]. Kasperovich, G. et al. Tailoring the strength of inconel 718: Insights into LPBF parameters and heat treatment synergy. Mater. Des. 250, 113627 (2025).
[16]. Teng, Q. et al. Composition modification and experimental verification of Hastelloy X superalloy with superior mechanical properties fabricated by laser powder bed fusion. J. Mater. Res. Technol. 41, 4757–4770 (2026).
[17]. Wang, Y. et al. Tailoring microstructure and mechanical properties of IN738LC fabricated by laser powder bed fusion through processing parameter optimization. Opt. Laser Technol. 188, 112887 (2025).
[18]. DebRoy, T. et al. Additive manufacturing of metallic components – Process, structure and properties. Prog. Mater. Sci. 92, 112–224 (2018).
[19]. Lin, S., Chen, K., He, W., Tamura, N. & Ma, E. Custom-designed heat treatment simultaneously resolves multiple challenges facing 3D-printed single-crystal superalloys. Mater. Des. 222, 111075 (2022).
[20]. Tucho, W. M., Cuvillier, P., Sjolyst-Kverneland, A. & Hansen, V. Microstructure and hardness studies of Inconel 718 manufactured by selective laser melting before and after solution heat treatment. Mater. Sci. Eng. A 689, 220–232 (2017).
[21]. Zhou, S., Liu, L., Yang, Y. & Lv, P. Effect of heat treatment on the microstructure and recrystallization of an SLM nickel-based superalloy. Mater. Today Commun. 39, 109253 (2024).
[22]. Lee, J. U., Kim, Y. K., Seo, S. M. & Lee, K. A. Effects of hot isostatic pressing treatment on the microstructure and tensile properties of Ni-based superalloy CM247LC manufactured by selective laser melting. Mater. Sci. Eng. A 841, 143083 (2022).
[23]. Bassini, E. et al. Effects of the solution and first aging treatment applied to as-built and post-HIP CM247 produced via laser powder bed fusion (LPBF). J. Alloys Compd. 905, 164213 (2022).